



Cite this: *Phys. Chem. Chem. Phys.*,
2018, 20, 18907

Received 6th June 2018,
Accepted 25th June 2018

DOI: 10.1039/c8cp03582b

rsc.li/pccp

Reliable and computationally affordable prediction of the energy gap of $(\text{TiO}_2)_n$ ($10 \leq n \leq 563$) nanoparticles from density functional theory†

Ángel Morales-García, * Rosendo Valero  and Francesc Illas *

The optical gap (O_{gap}) of a set of $(\text{TiO}_2)_n$ nanoclusters and nanoparticles with $n = 10$ –563 and different morphologies such as spherical, octahedral, lamellar, or tubular finite structures is investigated based on a relativistic all-electron description along with a numerical atomic centered orbital basis set. Two different functionals are used, PBE and PBE_x, the former corresponds to a standard implementation of the generalized gradient approximation (GGA) and the latter to a hybrid functional with 12.5% of Fock exchange which reproduces the band gap of bulk TiO_2 anatase and rutile. It is shown that the inclusion of exchange Fock in the PBE functional promotes a systematic energy gap opening of 1.25 eV relative to the PBE values. Remarkably, a linear correlation is found between PBE_x and PBE O_{gap} calculated values with concomitant similar correlations for the HOMO and LUMO orbital energies. However, it appears that PBE_x induces a larger downshift on the HOMO orbital than the upshift observed on the LUMO one. The fact that the PBE_x hybrid functional was shown to reproduce the experimental energy gaps of stoichiometric and reduced TiO_2 bulk phases leads to a suitable and practical way to successfully estimate O_{gap} of TiO_2 nanoparticles containing up to thousands of atoms with PBE_x precision from computationally affordable PBE calculations.

The water splitting breakthrough reported by Fujishima and Honda is one of the main discoveries that promoted the development of photocatalysis across a broad range of research areas, including especially environmental and energy-related fields.^{1–3} The photocatalytic properties of certain materials have been used with the ultimate goal of converting solar energy into chemical energy used either to oxidize or to reduce compounds, to obtain useful products including hydrogen and hydrocarbons, and to remove pollutants and bacteria from wall surfaces, either in air or in water environments.^{4–7} Among different photocatalysts investigated, titanium dioxide (TiO_2) is a fascinating material exhibiting

unique photocatalytic properties which are exploited in many technological applications due to its strong oxidizing abilities for the decomposition of organic pollutants, chemical stability, long durability, nontoxicity and low cost.^{2,8} The possibility to use sunlight for photocatalytic processes carries the promise to an almost inexhaustible and sustainable energy source and TiO_2 , in its many forms, is by far the most studied compound. However, the exceedingly large energy gap of TiO_2 implies that an earnest effort has to be put into understanding the electronic structure of TiO_2 nanoparticles to provide arguments for a rational design of photocatalysts with reduced band gaps. Many TiO_2 nanostructures with different morphologies such as spheres, nanorods, fibers, tubes, sheets, and interconnected architectures have been recently fabricated.^{9–13} Not surprisingly, the morphology and the size of the system are two aspects to control when aiming at optimizing its photocatalytic activity.¹⁴

Unfortunately, because of many technical problems, it is very difficult to rely on experiments to correlate the effect of size and shape to the electronic properties of TiO_2 nanosystems. On the other hand, computational modeling provides a reliable and unbiased approach to analyze the influence of these factors on the structural and electronic properties. However, the modelization of different morphologies (for a fixed composition) or compositions (for a fixed morphology) requires appropriate systems containing perhaps thousands of atoms. Recent works based on bottom-up^{15–17} and top-down¹⁸ models of TiO_2 nanoparticles have been reported showing that it is nowadays possible to approach the properties of large systems by means of first principles density functional theory (DFT) based calculations. These works have shown how electronic properties of TiO_2 finite systems, such as the optical gap (O_{gap}), corresponding to the lowest singlet to singlet excitation, and electronic gap (E_{gap}), defined as the difference between the vertical ionization potential and the electron affinity, evolve with the morphology of the material.^{15,18} The largest variations are, not surprisingly, observed in the quite small $(\text{TiO}_2)_n$ nanoclusters with $n < 30$.¹⁵ These fluctuations result from quantum confinement and atomic environments which are far enough away from the bulk atomic connections.

Departament de Ciència de Materials i Química Física & Institut de Química Teòrica i Computacional (IQTCUB), Universitat de Barcelona. c/Martí i Franquès 1, 08028 Barcelona, Spain. E-mail: francesc.illas@ub.edu, angel.morales@ub.edu

† Electronic supplementary information (ESI) available. See DOI: 10.1039/c8cp03582b

For fairly large nanoparticles of ~ 6 nm and containing more than one thousand atoms, the O_{gap} and E_{gap} values are larger than those predicted for the bulk phases using the same computational approach.¹⁸ Nevertheless, a monotonous trend on O_{gap} and E_{gap} converging to the bulk like values as the size increases is observed and it also concluded that $(\text{TiO}_2)_{84}$ nanoparticles can be considered at the onset of the so-called scalable regime where properties scale linearly with the size toward the bulk like limit. This behavior is systematically observed with a similar trend for semilocal and hybrid exchange–correlation functionals. The inclusion of the Fock exchange through PBE x (PBE¹⁹ with 12.5% Fock) and PBE0 (PBE with 25% Fock) leads to larger values of both O_{gap} and E_{gap} contribution and, in view of the results reported for bulk phases,²⁰ is expected to provide more accurate results even if the trends observed with the PBE functional are maintained. The origin of the up-shifts in the PBE calculated O_{gap} is associated to systematic errors as recently reported for a large database of extended solids.²¹ In particular, a linear correlation was found between the PBE and G_0W_0 calculated O_{gap} values, the latter matching nicely the experimental values. Note in passing that in the absence of excitons, O_{gap} and E_{gap} values in extended solids coincide. Interestingly, the above correlations indicate that the problem of predicting the band gap from standard DFT calculations arises from the incorrect assignment of the quasiparticle character to the Kohn–Sham energy levels. The correlation also indicates that taking the Kohn–Sham bands to estimate the band gap carries a systematic error that can be corrected by invoking this correlation. The question that naturally arises is whether this systematic error also holds for TiO_2 nanoparticles since in that case it would be possible to estimate the energy gap of sufficiently large nanoparticles that better mimic the synthesized ones.

In this communication, we investigate whether the correlation found for PBE and PBE x calculated O_{gap} values on periodic insulators or semiconductors, and hence between PBE and G_0W_0 and, consequently, between PBE and the experiment also, holds for TiO_2 finite systems. To this end we study many different morphologies such as spherical, octahedral, lamellar, or tubular finite structures (further structural details can be found in ref. 15 and 17). The O_{gap} is estimated from the HOMO–LUMO energy gap defined from the Kohn–Sham orbital energies since, even if it cannot be considered as a reliable approximation to this quantity, detailed studies at the G_0W_0 level of theory have shown that the trends are meaningful.²² A set of 75 different $(\text{TiO}_2)_n$ finite systems with n ranging from 10 to 286 units has been selected and classified into two groups attending to the number of TiO_2 units: (i) nanoclusters ($n \leq 40$) obtained by using a bottom-up approach based on a hybrid genetic algorithm¹⁷ and global optimization¹⁵ and (ii) nanoparticles ($n > 40$) which are obtained by using a top-down approximation¹⁸ *via* Wulff constructions.²³ Note that the top-down approach allows one to relate the shape of the nanoparticle with the area of the surfaces exposed concerning their relative stability.¹⁶ Rutile and anatase bulk phases were used to design nanoparticles containing up to 1689 atoms.²⁴ As an example, Fig. 1 compiles a set of six TiO_2 nanoclusters and

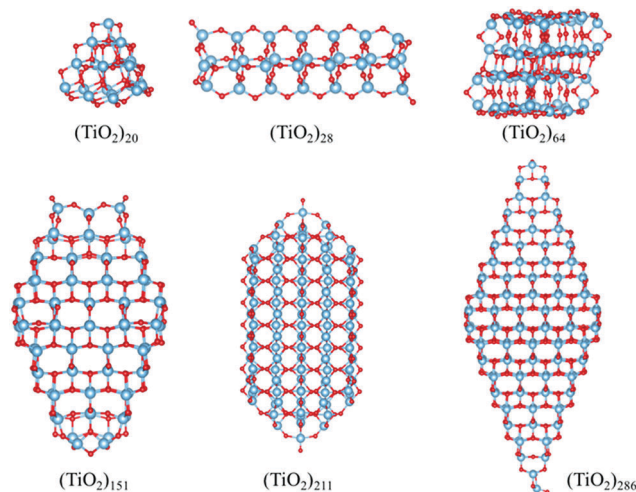


Fig. 1 Representative scheme of $(\text{TiO}_2)_n$ nanoclusters ($n = 20, 28$ and 64) and nanoparticles ($n = 151, 211$ and 286). Nanoclusters and nanoparticles are obtained by using bottom-up and top-down approaches, respectively. $(\text{TiO}_2)_{151}$ is structurally described as an anatase-type truncated octahedral nanoparticle. $(\text{TiO}_2)_{211}$ is a rutile-type polyhedral nanoparticle, and finally $(\text{TiO}_2)_{286}$ is also an anatase-type octahedral nanoparticle.

nanoparticles representing the rich variety of sizes and shapes analyzed in the present study.

Calculations reported in the present work for the series of nanoparticles described above explicitly include all electrons, and the electron density is described through a numerical atom-centered (NAO) orbital basis set, as implemented in the Fritz Haber Institute *ab initio* molecular simulations (FHI-aims) code which shows a linear scaling with the number of cores for systems composed of thousands of atoms.²⁵ The light grid and tier-1 basis set are selected which lead to a quality comparable to that corresponding to a Gaussian type orbital TZVP basis set.¹⁸ The convergence threshold for atomic forces in relaxation of TiO_2 nanoclusters and nanoparticles is set to 10^{-2} eV \AA^{-1} . Relativistic effects are also included through the zero-order regular approximation (ZORA).^{26,27}

We start with the analysis of the PBE or PBE x calculated O_{gap} values of TiO_2 nanoclusters ($n = 10$ – 40). Recall that within this size range O_{gap} depends strongly on the nanocluster morphology, which is clearly shown by the wide range of O_{gap} reported, 1.80–3.60 eV ($\Delta = 1.80$ eV), calculated by using the PBE functional. This variation on the O_{gap} value also affects TiO_2 nanocluster isomers with different morphologies. For instance, three different $(\text{TiO}_2)_{18}$ nanoclusters were analyzed reporting O_{gap} values running from 1.92 to 3.01 eV or similarly the case of other three different $(\text{TiO}_2)_{40}$ ones which go from 2.09 to 2.94 eV (see Tables S1 and S2 in the ESI[†]). PBE x results show similar tendencies, but the range of O_{gap} is quantitatively increased up to 3.01–4.87 eV ($\Delta = 1.86$ eV) due to the inclusion of the Fock contribution. In the light of the PBE x hybrid functional containing the appropriate percent of exchange Fock contribution, the O_{gap} values are significantly larger than those of anatase and rutile bulk phases, 3.2 and 3.0 eV, respectively (see Tables S1 and S2 in the ESI[†]). These large differences depending on the TiO_2 nanocluster

are associated with the system size, which is well away from the bulk limit region. This is consistent with previous findings that indicate that very large TiO_2 nanoparticles composed of hundreds of TiO_2 units are required to obtain models with electronic properties close to the bulk like one, consistent with the experimental evidence.

Octahedral $(\text{TiO}_2)_n$ nanoparticles with $n = 84, 165$ and 286 and truncated octahedral ones with $n = 78, 97$ and 151 , both terminated so as to exhibit the most stable (101) and (101)/(001)¹⁸ surfaces of TiO_2 anatase, respectively, are considered (see Fig. 1 and Table S3 in the ESI†). For this set of nanoparticles, the PBE O_{gap} value tends to the anatase PBE bulk phase value by increasing the nanoparticle size ($n \sim \infty$). The TiO_2 nanoparticles with octahedral shape have a PBE O_{gap} value of 2.52 eV for $(\text{TiO}_2)_{84}$, and a decreased value of 2.32 eV for $(\text{TiO}_2)_{286}$. Using the PBEx functional shifts these values up to 3.56 and 3.46 eV, respectively, values converging to the PBEx anatase band (3.2 eV), although still large. An analogous tendency is observed for the TiO_2 truncated octahedral shape, where the PBE O_{gap} values of 2.46 and 2.38 eV are predicted for $(\text{TiO}_2)_{78}$ and $(\text{TiO}_2)_{151}$, respectively, which become 3.61 and 3.51 eV when using the PBEx functional (see Table S3 in the ESI†). The case of rutile nanoparticles ($n = 86, 111$ and 211) is more complex because the (110), (101) and (100) surfaces must be considered for designing the nanoparticles.²⁴ The PBE O_{gap} values for $(\text{TiO}_2)_{111}$ and $(\text{TiO}_2)_{211}$ are 1.71 and 1.66 eV, respectively, whereas the PBEx values are 2.76 and 2.71 eV. The latter values tend to the energy gap of the rutile bulk phase (3.0 eV). In summary, large TiO_2 nanoparticles visualize clearly the trend of O_{gap} towards the bulk like regime, whereas TiO_2 nanoclusters behave differently, as expected. Note that the energy gap of anatase- and rutile- TiO_2 nanoparticles is overestimated and underestimated from the bulk band gap, respectively, due to the quantum confinement effects in combination with surface effects in the case of rutile- TiO_2 nanoparticles.²⁴

Next we analyze the correlation between the PBE and PBEx calculated O_{gap} values which is reported in Fig. 2. A quantitatively enough linear correlation between both sets of calculated O_{gap} values emerges as in eqn (1),

$$O_{\text{gap}}(\text{PBEx}) = 0.995 \cdot O_{\text{gap}}(\text{PBE}) + 1.253 \quad (1)$$

with a regression coefficient of 0.98. This correlation confirms that the Fock contribution to the exchange induces a systematic opening of the Kohn–Sham HOMO and LUMO orbital energies for the set of TiO_2 nanoclusters and nanoparticles. Interestingly enough, this systematic effect is observed for any nanoparticle with any morphology and any size. The offset value of 1.25 eV is consistent with the existence of a systematic deviation on the PBE results for O_{gap} that we attribute to the interpretation of Kohn–Sham orbital energies as quasiparticle excitation. It should be pointed out that this linear correlation allows one to predict PBEx O_{gap} values of any TiO_2 nanoparticle composed of hundreds/thousands of TiO_2 units where the use of hybrid functionals is computationally unfeasible. Thus, we provide here a suitable way to predict the O_{gap} of large TiO_2 nanoparticles with a PBEx precision by just carrying out a single point calculation with the PBE functional. Moreover, in view of

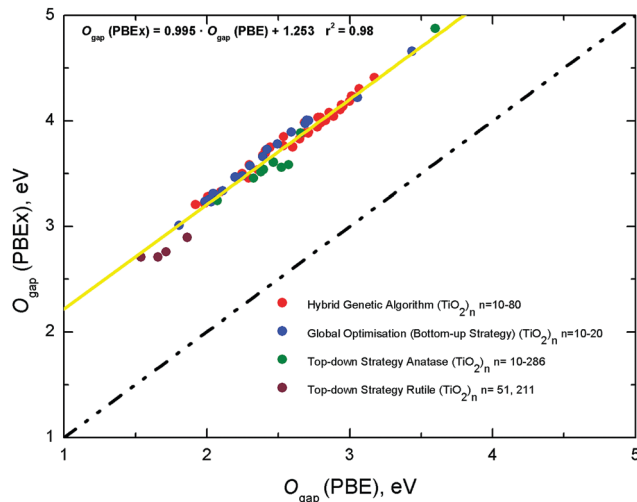


Fig. 2 Correlation between $O_{\text{gap}}(\text{PBEx})$ and $O_{\text{gap}}(\text{PBE})$ for the set of 75 $(\text{TiO}_2)_n$ nanoclusters/nanoparticles. O_{gap} is taken as the HOMO–LUMO gap which corresponds to the Kohn–Sham orbital energies. The point-dashed line corresponds to an ideal correlation $y = x$ and the yellow line to the linear fitting.

the (by construction) coincidence between PBEx and the experiment for bulk phases, it is possible to argue that PBE O_{gap} and eqn (1) will provide a reliable value of this important quantity. For instance, for the anatase $(\text{TiO}_2)_{455}$ and rutile $(\text{TiO}_2)_{563}$ nanoparticles, the PBE O_{gap} values reported in Table 1 plus eqn (1) lead to predicted PBEx O_{gap} values of 3.46 and 2.94 eV for $(\text{TiO}_2)_{455}$ and $(\text{TiO}_2)_{563}$, respectively. The explicit calculation of these particles at the PBEx level remains unfeasible, or too costly, even with appropriate codes and the modern highly parallel supercomputers with thousands of cores.

To end up the discussion, we focus on the effect of the Fock exchange in the PBEx hybrid functional on the energy of HOMO and LUMO orbitals. Obviously, the opening of an energy gap in going from PBE to PBEx is accompanied by changes in the energy of Kohn–Sham orbitals. Fig. 3 depicts the PBEx HOMO and LUMO orbital energies against the PBE ones. As in the case of O_{gap} (Fig. 2), a linear correlation is found for the HOMO orbital energy as in eqn (2),

Table 1 O_{gap} for anatase $(\text{TiO}_2)_{455}$ and rutile $(\text{TiO}_2)_{563}$ nanoparticles calculated by using the PBE functional. The predicted O_{gap} with a PBEx precision is calculated by using eqn (1)–(3). $|\Delta|$ stands for the difference between the predicted $O_{\text{gap}}(\text{PBEx})$ by using eqn (1) and that predicted by using the estimated PBEx LUMO–HOMO difference from eqn (2) and (3), respectively

		Anatase $(\text{TiO}_2)_{455}$	Rutile $(\text{TiO}_2)_{563}$
PBE	HOMO	−7.465	−7.247
	LUMO	−5.253	−5.558
	O_{gap}	2.212	1.689
Predicted PBEx	HOMO eqn (2)	−8.308	−8.093
	LUMO eqn (3)	−4.919	−5.233
	O_{gap}	3.389	2.859
	O_{gap} eqn (1)	3.465	2.942
	$ \Delta $ (O_{gap})	0.076	0.083

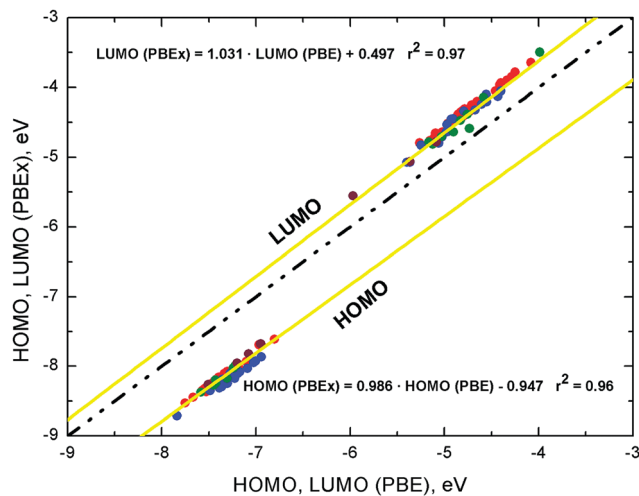


Fig. 3 Correlation between HOMO and LUMO Kohn–Sham orbital energies of PBEx and PBE functionals for the set of 75 $(\text{TiO}_2)_n$ nanoclusters/nanoparticles. The color scheme follows the same notation as reported in Fig. 2 inset. The point-dashed line corresponds to an ideal correlation $y = x$ and the yellow lines to linear fittings.

$$\text{HOMO (PBEx)} = 0.986 \cdot \text{HOMO (PBE)} - 0.947 \quad (2)$$

with a regression coefficient of 0.96, consistent with a second linear correlation for the LUMO orbital energy as in eqn (3),

$$\text{LUMO (PBEx)} = 1.031 \cdot \text{LUMO (PBE)} + 0.497 \quad (3)$$

with a regression coefficient of 0.97. The slope of both fittings is close enough to 1 so as to conclude that the effect of Fock exchange is larger for the HOMO orbitals than for the LUMO ones. This is clearly observed in Fig. 3 by the shifting of both linear tendencies with respect to the ideal correlation; the HOMO correlation is further away from it than the LUMO one. From eqn (2) and (3) one can predict the PBEx energy of the HOMO and LUMO orbitals as reported in Table 1 for $(\text{TiO}_2)_{455}$ and $(\text{TiO}_2)_{563}$ nanoparticles introduced earlier. The resulting O_{gap} values are 3.39 and 2.86 eV for $(\text{TiO}_2)_{455}$ and $(\text{TiO}_2)_{563}$, respectively. Note that the energy gap difference between these O_{gap} values and those obtained by using eqn (1) is less than 0.1 eV (see Table 1), showing the consistency between both correlations to estimate O_{gap} .

In summary, the optical gap (O_{gap}) in TiO_2 nanoclusters and nanoparticles has been investigated by making use of all electron relativistic DFT based calculations employing the PBE semilocal functional and the hybrid PBEx containing 12.5% of Fock exchange. The present results provide further evidence that O_{gap} is a morphology-dependent property and its value depends on the system size and the atomic environments of Ti and O atoms. This dependency is larger in small clusters where there is a noted variation on the atomic environments for similar isomers.²² On the other hand, small $(\text{TiO}_2)_n$ nanoclusters ($n = 10\text{--}40$) have O_{gap} values much larger than the corresponding bulk values predicted with the same functional. These large differences are reduced by moving from nanoclusters

to nanoparticles which show a bulk like trend consistent with previous studies.¹⁸

The present study shows that irrespective of the size and morphology, the PBEx hybrid functional induces a systematic gap opening of 1.25 eV for the set of TiO_2 nanoclusters and nanoparticles investigated. The linear correlation found between PBEx and PBE O_{gap} values allows one to predict PBEx quality energy gaps for those TiO_2 finite systems whose dimensionality makes the explicit calculation with hybrid functionals unaffordable. We have further investigated the accuracy of the correlation by fitting the energy gaps for nanoparticles with $n < 80$ only and predicting those of the largest nanoparticles. The comparison between the calculated and predicted PBEx O_{gap} values shows a mean absolute error (MAE) below 0.2 eV (see Fig. S1, S2 and Table S5 in the ESI†). Similar linear trends are observed on HOMO and LUMO orbitals and hence, both orbital energies can be predicted following their trends shown in eqn (2) and (3). The percent of Fock exchange in the hybrid functional has a higher contribution to the HOMO orbitals than to the LUMO ones, which promotes a larger downshift on the HOMO orbital than the upshift on the LUMO one.

Results in the present work show that is possible to obtain a PBEx description of the electronic structure of TiO_2 nanoparticles from the computationally affordable PBE results. Note that the PBE functional does not describe appropriately the electron localization and polarons in stoichiometric and non-stoichiometric nanoparticles requiring more sophisticated approaches such as hybrid functionals for an appropriate description. It also suggests that similar correlations will exist with other hybrid functionals such as the well-known B3LYP, and PBE0 and HSE06 due to the systematic opening of the energy gap that the inclusion of a percent of Fock exchange generates.^{18,22,28} This is in line with previous work highlighting the existence of a similar correlation for the electronic gap as predicted from PBE or G_0W_0 calculations.²¹ Taken together, one can firmly affirm that well-known deviations in the electronic structure properties of nanosized and bulk semiconducting materials predicted by functionals within the generalized gradient approximation relative to those predicted from more accurate hybrid functional or many body-based GW approaches are systematic and as such it should be possible to come out with improved and more accurate density functionals.

Conflicts of interest

There are no conflicts to declare.

Acknowledgements

The authors acknowledge funding from the Spanish *Ministerio de Economía y Competitividad* (MEC) CTQ2015-64618-R grant, partly from *Generalitat de Catalunya* grants 2017SGR13 and XRQTC, and the NOMAD Center of Excellence project, which received funding from the European Union's Horizon 2020 Research and Innovation Programme under grant agreement

no. 676580. A. M.-G. thanks the Spanish MEC for the *Juan de la Cierva* (FJCI-2015-23760) postdoctoral grant. F. I. acknowledges additional support from the 2015 ICREA Academia Award for Excellence in University Research. Computational time at the MareNostrum supercomputer has been provided by the Barcelona Supercomputing Centre (BSC) through grants from *Red Española de Supercomputación* (RES) and the EXCIPHOCAT project under grant no. 2016163940 of the Partnership for Advanced Computing in Europe (PRACE).

References

- 1 A. Fujishima and K. Honda, *Nature*, 1972, **238**, 37–38.
- 2 K. Hashimoto, H. Irie and A. Fujishima, *Jpn. J. Appl. Phys.*, 2005, **44**, 8269–8285.
- 3 A. Fujishima, X. Zhang and D. A. Tryk, *Surf. Sci. Rep.*, 2008, **63**, 515–582.
- 4 A. Ryu, *J. Photochem. Photobiol., C*, 2010, **11**, 179–209.
- 5 T. Inoue, A. Fujishima, S. Konishi and K. Honda, *Nature*, 1979, **277**, 637–638.
- 6 L. Caballero, K. A. Whitehead, N. S. Allen and J. Verran, *J. Photochem. Photobiol., A*, 2009, **202**, 92–98.
- 7 K. Sunada, T. Watanabe and K. Hashimoto, *Environ. Sci. Technol.*, 2003, **37**, 4785–4789.
- 8 H. Xu, S. Ouyang, L. Liu, P. Reunchan, N. Umezawa and J. Ye, *J. Mater. Chem. A*, 2014, **2**, 12642–12661.
- 9 J. S. Chen, Y. L. Tan, C. M. Li, Y. L. Cheah, D. Luan, S. Madhavi, F. Y. C. Boey, L. A. Archer and X. W. Lou, *J. Am. Chem. Soc.*, 2010, **132**, 6124–6130.
- 10 X. Feng, J. Zhai and L. Jiang, *Angew. Chem., Int. Ed.*, 2005, **44**, 5115–5118.
- 11 Y. Cheng, W. Huang, Y. Zhang, L. Zhu, Y. Liu, X. Fan and X. Cao, *CrystEngComm*, 2010, **12**, 2256–2260.
- 12 J. M. Macak, M. Zlamal, J. Krysa and P. Schmuki, *Small*, 2007, **3**, 300–304.
- 13 T. Shibata, N. Sakai, K. Fuduka, Y. Ebina and T. Sasaki, *Phys. Chem. Chem. Phys.*, 2007, **9**, 2413–2420.
- 14 X. Chen and S. S. Mao, *Chem. Rev.*, 2007, **107**, 2891–2959.
- 15 O. Lamiel-García, A. Cuko, M. Calatayud, F. Illas and S. T. Bromley, *Nanoscale*, 2017, **9**, 1049–1058.
- 16 D. Cho, K. C. Ko, O. Lamiel-García, S. T. Bromley, J. Y. Lee and F. Illas, *J. Chem. Theory Comput.*, 2016, **12**, 3751–3763.
- 17 M. Chen and D. A. Dixon, *Nanoscale*, 2017, **9**, 7143–7162.
- 18 O. Lamiel-García, K. C. Ko, J. Y. Lee, S. T. Bromley and F. Illas, *J. Chem. Theory Comput.*, 2017, **13**, 1785–1793.
- 19 J. P. Perdew, K. Burke and M. Ernzerhof, *Phys. Rev. Lett.*, 1996, **77**, 3865–3868.
- 20 K. C. Ko, O. Lamiel-García, J. Y. Lee and F. Illas, *Phys. Chem. Chem. Phys.*, 2016, **18**, 12357–12367.
- 21 A. Morales-García, R. Valero and F. Illas, *J. Phys. Chem. C*, 2017, **121**, 18862–18866.
- 22 A. Morales-García, R. Valero and F. Illas, *J. Chem. Theory Comput.*, 2017, **13**, 3746–3753.
- 23 G. Wulff, *Z. Kristallogr.*, 1901, **34**, 449–530.
- 24 K. C. Ko, S. T. Bromley, J. Y. Lee and F. Illas, *J. Phys. Chem. Lett.*, 2017, **8**, 5593–5598.
- 25 V. Blum, R. Gehrke, P. Hanke, P. Havu, V. Havu, X. Ren, K. Reuter and M. Scheffler, *Comput. Phys. Commun.*, 2009, **180**, 2175–2196.
- 26 C. Chang, M. Pelissier and M. Durand, *Phys. Scr.*, 1986, **34**, 394–404.
- 27 E. van Lenthe, R. van Leeuwen, E. J. Baerends and J. G. Snijders, *Int. J. Quantum Chem.*, 1994, **57**, 281–293.
- 28 M. K. Y. Chan and G. Ceder, *Phys. Rev. Lett.*, 2010, **105**(196403), 1–4.